Fast Thermo-Optical Excitability in a Two-Dimensional Photonic Crystal

A. M. Yacomotti,[1,*] P. Monnier,[1] F. Raineri,[1] B. Ben Bakir,[2] C. Seassal,[2] R. Raj,[1] and J. A. Levenson[1]

[1]*Laboratoire de Photonique et de Nanostructures (CNRS UPR 20), Route de Nozay, 91460 Marcoussis, France*

[2]*Laboratoire d'Electronique Optoélectronique et Microsystèmes (CNRS UMR 5512), 36 av Guy de Collongue, 69134 Ecully Cedex, France*

(Received 22 March 2006; published 5 October 2006)

We experimentally demonstrate excitability in a semiconductor two-dimensional photonic crystal. Excitability is a nonlinear dynamical mechanism underlying pulselike responses to small perturbations in systems possessing one stable state. We show that a band-edge photonic crystal resonator exhibits class II excitability, resulting from the nonlinear coupling between the high-Q optical mode, the charge-carrier density, and the fast (sub-μs) thermal dynamics. In this context, the critical slowing down of the electro-optical dynamics close to the excitable threshold can delay the optical response by an amount comparable to the duration of the output pulse (5 ns). The latter results from a short thermal dynamical excursion along a high local intensity manifold of the phase space.

DOI: 10.1103/PhysRevLett.97.143904 PACS numbers: 42.70.Qs, 05.45.−a, 42.65.Sf

Excitability underlies dynamical processes leading to spiking behavior in many biological (neurons and cardiac tissue), chemical (Belousov-Zhabotinsky reaction) as well as physical systems (driven mechanical pendulum, lasers, and amplifiers) [1]. An excitable system possesses only one stable state and reacts to an external perturbation in the form of all-or-nothing pulse responses, depending on whether the perturbation is above or below a certain threshold. The first studies on excitability come from neuroscience in an effort to classify neural dynamics [2]. Only recently have there been experimental demonstrations of excitability in nonlinear optical cavities. These studies concerned semiconductors lasers with optical feedback [3], gas and solid state lasers with saturable absorber [4], as well as thermo-optical pulsation in broad-area semiconductor amplifiers [5,6]. Excitability offers interesting prospects for applications in all-optical circuits, such us clock recovery and pulse reshaping [7].

An excitable system presents a transition to self-sustained oscillations as one control parameter is varied. In particular, the so-called class II excitability is characterized by a transition to oscillations within a nonzero narrow frequency band [8]. In this class, two distinct time scales are present: the fast one is responsible for the firing of the excitable pulse, and the slow one determines the full recovery to the quiescent state. This is the case of the optical amplifier with injected signal, where fast and slow variables are carrier density and temperature, respectively. In standard resonators, as the one used in Ref. [5], the time scale for thermal relaxation is of the order of ms. In microphotonic resonators such as microdisks or photonic crystals (PCs), the thermal relaxation time becomes much faster, due to the small dimensions playing a role in heat diffusion. In a recent work, self-induced optical modulation of the transmission through a high quality factor (Q) microdisk was reported [9]; the thermal recovery there is of the order of μs. Furthermore, recent studies on optomechanical oscillations driven by radiation pressure have also shown two time-scale self-sustained oscillations in ultrahigh Q microtorus [10]. More generally, the world of microphotonic devices concerns high and ultrahigh Q resonators [11] which, under light injection, enhance carrier absorption and radiation pressure thus involving ubiquitous thermal or mechanical dynamical effects, respectively. Here, we take advantage of thermal effects in order to control light in a fast excitable regime.

The aim of this work is twofold: (i) We demonstrate excitability in a high-Q bidimensional (2D) PC resonator; (ii) we show that the parameters can be chosen such that the output pulse duration, determined by a thermal excursion in phase space, becomes as short as the electronic relaxation time, i.e., of the order of ns. This provides a nonlinear dynamical basis for all-optical control of light, such as a mean of realizing optical delay lines.

Our 2DPC sample is sketched in Fig. 1(a). A graphite lattice of cylindrical air holes is patterned into a 20 μm $\times$ 20 μm, 240-nm-thickness InP slab through a silica mask obtained by electron beam lithography followed by reactive ion etching. The lattice constant and hole diameter are 775 and 230 nm, respectively. The InP slab contains 4 quantum wells (QWs) of $InAs_{0.65}P_{0.35}$ [12], whose luminescence is centered at 1500 nm. The heterostructure is then transferred onto a SiO_2-Si Bragg mirror, including 3 pairs of $\lambda/(4n)$ layers, on a silicon wafer by SiO_2-SiO_2 wafer bonding. The top medium is air.

The 2DPC is designed in order to exhibit a flat band edge at the Γ point (in-plane wave vector equals zero) around 1550 nm (see band structure in Ref. [13]). As a result, light can be coupled resonantly into this low group velocity Bloch mode when it is incident normally to the PC surface. It has been shown elsewhere [14] that this type of structure can be seen as an equivalent resonator whose Q factor is determined both by the curvature of the photonic band and the radiative losses in the vertical direction. In our particular case, the Q factor is limited by these losses. In order to decrease them, a Bragg mirror is positioned

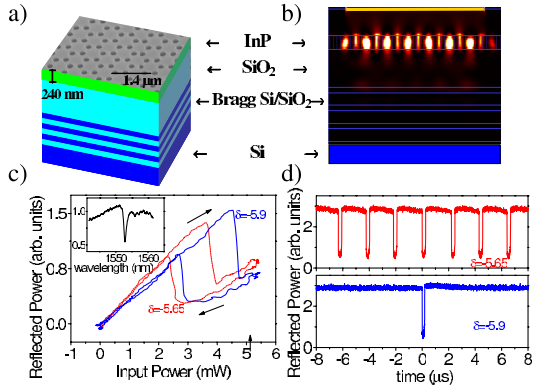

FIG. 1 (color online). (a) Sketch of the 2DPC (scanning electron microscopy image of the graphite lattice on top). (b) Cross-section distribution of the electromagnetic energy from a finite-difference time domain 3D numerical simulation of the real structure. The horizontal line on the top represents the extension of the injected CW resonant plane wave. Note the confinement in the InP slab. (c) Experimental bistability hysteresis cycles obtained with 200-ns-width, 400-μs-period pulses with $\lambda_{\text{in}} = 1550.54$ nm ($\delta = -5.9$, solid line) and $\lambda_{\text{in}} = 1550.64$ nm ($\delta = -5.65$, dotted line). Inset: reflectivity spectrum (vertical scale is in arbitrary units). (d) Reflected power as a function of time under CW injection for $\delta = -5.65$ (top trace) and $\delta = -5.9$ (bottom trace); injected power is 5.1 mW [vertical arrow in (c)].

$3\lambda/4n$ below the 2DPC [15]. In addition, as can be seen in Fig. 1(b), this configuration ensures that light is strongly confined in the vertical direction in the PC slab. For this reason, all the nonlinear processes at the heart of the phenomena studied in this Letter are supposed to take place in this layer. The reflectivity spectrum obtained from femtosecond-probe pulses centered at 1550 nm is shown in the inset of Fig. 1(c). A linear resonance with FWHM of $\Delta\lambda_{\text{lin}} = 0.8$ nm is observed, centered at $\lambda_{\text{lin}} = 1552.9$ nm. This resonance blueshifts and narrows as 810 nm pump pulses are injected coincidently with the probe pulses [12]. In particular, transparency is reached at ~ 1 kW/cm^2 pump intensity ($\lambda_{\text{tr}} = 1548.9$ nm and $\Delta\lambda_{\text{tr}} = 0.3$ nm). The Q factor at transparency yields $Q_{\text{tr}} = 5160$, and the associated photon lifetime $\tau_{\text{tr}} = 4.2$ ps. The electronic recombination time scale was measured to be $\tau_r = 275$ ps.

In a recent work [13], we demonstrated bistable operation as 4 -mW-peak power (5 μm diameter beam waist), 200-ns-width pulses were injected at the blue side of the resonance. Under these conditions, hysteresis cycles are shown for two normalized detunings, $\delta \equiv (\lambda_{\text{in}} - \lambda_{\text{lin}})/(\Delta\lambda_{\text{lin}}/2) = -5.65$ and -5.9, in Fig. 1(c). Thermal effects are minimized due to the short-pulse-low duty cycle modulation. Now we turn off this modulation. In absence of thermal effects, a stable state corresponding to the low reflectivity would be observed for high enough CW power injection, for instance, $P_{\text{in}} = 5.1$ mW. Instead, what *is* observed is self-sustained oscillations for $\delta = -5.65$ [Fig. 1(d), top trace] and a quasistable state with noise-triggered downward pulses for $\delta = -5.9$ [Fig. 1(d), bottom trace]. In the following we will demonstrate that the latter corresponds to excitable behavior.

For testing excitability, the system is prepared with $\delta = -5.75$ where the stable state corresponds to high reflected power [Fig. 1(d), bottom trace]. We perturb this state by injecting 12.5μs-period, 60-ps-width pulses at $\sim$800 nm. Since this duration is much shorter than the electronic lifetime, and since these pulses are absorbed in the quantum barriers, the perturbation can be seen as a kick in carrier density. For perturbation energies less than $U_p = 1.9$ pJ, no output pulse is observed. However, $U_p \geq 1.9$ pJ excites a 300-ns-width pulse in the reflected signal. This output remains essentially invariant for a further increase of the perturbation energy [Fig. 2(a)]. Therefore, the system is excitable. In addition, the power spectrum of the self-sustained oscillations shown in Fig. 1(d) (top trace) gives a sharp fundamental peak at $f = 0.5$ MHz, corresponding to the 2 μs pulse period. This builds confidence in class II excitability, with a slow time scale of ~ 1 μs.

Further decreasing the detuning reduces the excitable pulse duration dramatically, at the cost of increased threshold. In Fig. 2(b), for $\delta = -6.5$, the output pulse has a width of 3 ns. Next, we address the issue of modulation bandwidth. Even though the long recovery time is 1 μs, we can periodically perturb the system at much higher repetition rates without significant loss of contrast. This is due to the nonlinear dynamical nature of the relaxation oscillator. Note that a linear system with a relaxation time of 1 μs would keep only 1% of its full contrast when modulated at 100 MHz. In Fig. 2(c) we plot the time traces for different

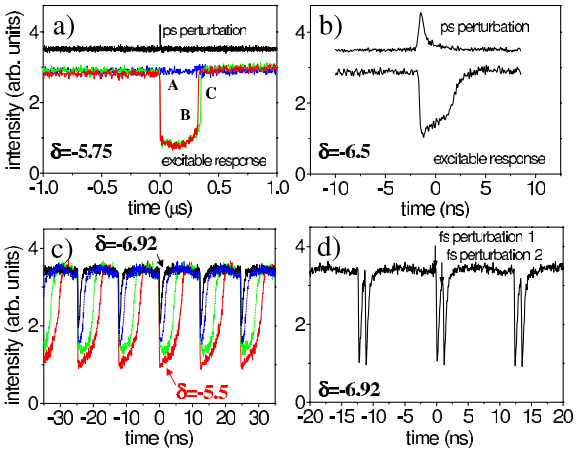

FIG. 2 (color online). (a) Excitable responses (bottom traces: >5 GHz bandwidth photodiode measurement) to 60-ps-width, 80-KHz-repetition rate pulse perturbations (top trace: avalanche photodiode measurement) with $U_p = 1.6$ pJ (label A), 1.9 pJ (label B), and 2.5 pJ (label C) ps-pulse energies; $\delta = -5.75$. (b) Fast output pulses with $\delta = -6.5$ and $U_p = 7.4$ pJ. (c) Fast modulation test with 100-fs-width, 80-MHz-repetition rate pulses. From longest to shortest output pulse: $\delta = -5.5, -6, -6.5, -6.92$; $U_p = 6$ pJ. (d) Bandwidth limit test, two pulse trains as in (c) delayed by 1 ns; $\delta = -6.92$; $U_{p,1} = 15$ pJ and $U_{p,2} = 6$ pJ.

detuning and 100-fs-duration, 80-MHz-repetition rate perturbation pulses. It can be observed that the excitable system can still lock 1:1 to the input pulses for the shorter response, while keeping more than 60% of the full contrast. In order to explore the bandwidth modulation -limit, we inject two delayed perturbation pulse trains at a 80 MHz repetition rate. High-contrast response pulses are still fired with 1 ns time delay between perturbations [Fig. 2(d)].

This type of excitability can be explained by considering a two time-scale dynamics: (slow) thermal effects coupled to (fast) optoelectronic ones. If a perturbation kicks the system from the high to the low reflectivity branch in the hysteresis cycle, then heating is enhanced, shifting the hysteresis cycle to higher injection powers. Therefore, a jump back to the high reflectivity state is possible, with a subsequent cooling, giving rise to a closed dynamical cycle at the origin of a downwards pulse. The main features of this process can be captured by a mean-field model of the slowly varying amplitude of the electromagnetic field (E) and carriers (N) in a single-mode high-Q optical resonator, in the presence of optical injection [16] and thermal effects [6,17]:

$$\frac{dE}{dt} = -E(1 + i\theta) + (1 - i\alpha)(N - N_t)E + E_I, \quad (1)$$

$$\frac{dN}{dt} = -\gamma[N + (N - N_t)|E|^2], \quad (2)$$

$$\frac{d\theta}{dt} = -\gamma_{\text{th}}\{\theta - \theta_0 + cE_I[\text{Re}(E) - |E|^2]\}. \quad (3)$$

Normalizations are such that $|E|^2 = I/I_{\text{sat}}$, where I is the circulating intensity in the resonator and I_{sat} the saturation intensity; N is normalized to the carrier density at transparency divided by N_t, the latter being the ratio between QW absorption and optical losses; time is normalized to $2\tau_c$, where τ_c is the photon lifetime of the cavity at transparency (corresponding to the experimental τ_{tr}) and gives the optical losses rate. The parameter α is the ratio between the real and the imaginary parts of the differential susceptibility at the central frequency of the optical resonance [18]; $\gamma = 2\tau_c/\tau_r$; $\theta \equiv (\omega_c - \omega_{\text{in}})(2\tau_c)$, where ω_c is the cavity mode at transparency and ω_{in} the injection frequency; $E_I = Q_c I_{\text{in}}/\pi I_{\text{sat}}$, where I_{in} is the external injected intensity and Q_c the quality factor. The last term in Eq. (3) comes from an energy balance between incoming, reflected, and transmitted power; i.e., the thermal index change is given by $\Delta n/n_0 = \mathcal{A}(|E_I|^2 - |E_r|^2 - |E|^2)$, where we have neglected spontaneous emission. We define $\gamma_{\text{th}} = 2\tau_c/\tau_{\text{th}}$ as the thermal relaxation rate [19] and $c \equiv 4\tau_{\text{th}}\mathcal{A}Q_c$.

We perform numerical integrations of Eqs. (1)–(3) with fixed parameters $\gamma = 0.03$, $\gamma_{\text{th}} = 10^{-5}$, and $N_t = \Delta\lambda_{\text{lin}}/\Delta\lambda_{\text{tr}} - 1 \sim 1$. Control parameters are E_I, which we fix to $E_I = \sqrt{25P_0}$ [20], where $P_0 \equiv (1 + N_t)^3/(\alpha N_t)$, and $\delta_0 = (\theta_0 - \alpha N_t)/(1 + N_t)$, the detuning with respect to the linear resonance.

Steady state solutions are given by the intersection of nullclines, i.e., curves in phase space defined by $d/dt = 0$. These are shown in the (N, δ) phase portraits of Fig. 3. Figure 3(a) shows the saturated, high local intensity-stable state solution for the absence of thermal coupling, i.e., $c = 0$, and initial detuning $\delta_0 = -3.2$. We relate this operation point to the experimental one shown in Fig. 1(c): the resonator is being injected outside the hysteresis loop, on the saturated (low reflectivity) branch. For $c > 0$ (thermal redshift) large enough, say, $c = 6$, the $d(\theta, E)/dt = 0$ nullcline [dotted lines in Figs. 3(a), 3(b), 3(d), and 3(e)] shifts and bends, giving one unstable fixed point solution and a stable limit cycle [Figs. 3(b) and 3(c)]: the relaxation oscillations, in good agreement to those of Fig. 1(d).

Decreasing the detuning to $\delta_0 = -3.35$, the fixed point becomes stable (Hopf bifurcation) and the system presents excitability. Kicking carrier density above the threshold, given by the middle branch of the $d(N, E)/dt = 0$ nullcline

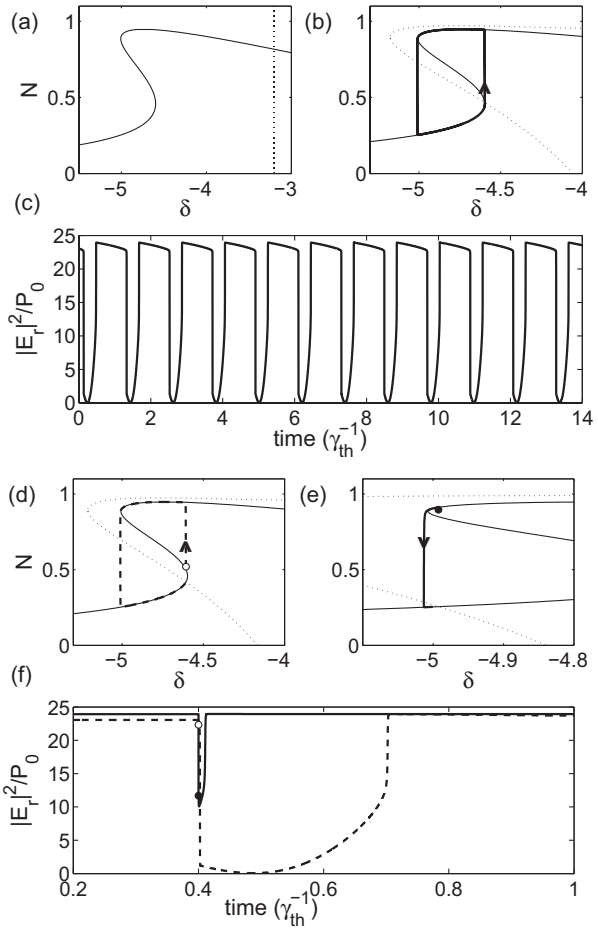

FIG. 3. Phase portraits and time traces of the reflected power ($E_r = E_I - E$) for (a) $\delta_0 = -3.2$ and $c = 0$ (no thermal effects); (b),(c) $c = 6$ (self-sustained oscillations); (d),(f) (dashed line) $\delta_0 = -3.35$, with perturbation $\Delta N = 0.1$ (slow excitability); (e),(f) (thick line) $\delta_0 = -4.225$, with perturbation $\Delta N = 0.65$ (fast excitability). Circles indicate the values of the variables $10 \times 2\tau_c$ after the perturbations. x-axis unit in time traces is $\tau_{\text{th}} = 0.84\ \mu$s.

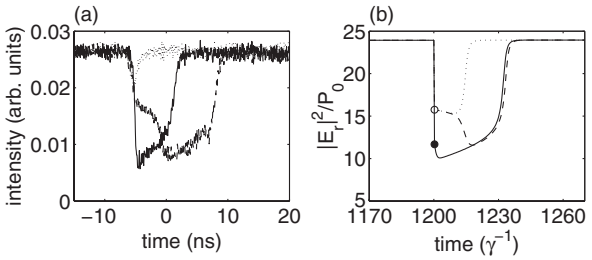

FIG. 4. (a) 60-ps-width pulse perturbation with $U_p = 5.5$ pJ (dotted line, below threshold), $U_p = 6.125$ pJ (dashed line, above and close to threshold), and $U_p = 9.3$ pJ (solid line, above threshold); $\delta = -6.875$ and $P_{\text{in}} = 5.42$ mW. (b) Numerical simulations with $\Delta N = 0.603\,004$ (dotted line, below threshold), $\Delta N = 0.603\,005$ (dashed line, above and close to threshold), $\Delta N = 0.65$ (solid line, above threshold); $\delta = -4.225$ [same as Fig. 3(e)]. x-axis unit is $\tau_r = 280$ ps.

[the S-shaped one in Figs. 3(a), 3(b), 3(d), and 3(e)], ejects the trajectory up in phase space, which rapidly collapses to the upper branch (τ_r-time scale), moves slowly towards more negative detuning (τ_{th}-time scale), jumps down to the bottom branch, and relaxes back to the initial state [Figs. 3(d) and 3(f)].

As in the experimental case [Figs. 2(b) and 2(c)], further decrease of initial detuning (to $\delta_0 = -4.225$) yields shorter reflectivity pulses. The stable state now locates close to the δ value at the left kink of the S-shaped nullcline [Fig. 3(e)]. Warming up has the same rate as before, but now the portion of the upper branch of the S-shaped nullcline to be slipped is much smaller compared to Fig. 3(d).

A most striking feature of our fast excitable 2DPC is that fast pulses arising from short thermal excursions can approach the carrier dynamics in a very specific situation called critical slowing down. Indeed, kicking the system close to the threshold slows down the optical response since the excitable threshold is a slow flow region of the phase space, a separatrix of all-or-none responses. In terms of the phase space structure, this corresponds to perturbations bringing trajectories close to the middle branch of the S nullcline of Fig. 3(e), which is a set of a unstable equilibrium points of the system without thermal coupling. Figure 4 shows three responses in the fast regime for perturbation energies below, close to, and above the excitable threshold, both experimental and theoretical. Above threshold the response takes place right after the perturbation, while close to threshold there is a time delay to the maximum of the response of about the duration of the low reflectivity state (5 ns). This constitutes an excitable mechanism for all-optical delay. The above-threshold experimental response is shorter compared to the theoretical one. Indeed, the pulse perturbation also induces a small heat injection due to nonradiative relaxation towards the semiconductor band edge. This additional heat, not included in our model, may kick δ in the early stage, thus "compressing" the output pulse.

In conclusion, we have demonstrated excitability in a 2DPC. This results from thermo-optical dynamics and was tested with short-light pulses. Theoretically, a mean-field model was able to reproduce the observed dynamical behaviors. The thermal time scale is 1 μs, leading to excitable pulses as short as 1 ns due to short thermal excursions in phase space. As a result, on-threshold short-pulse excitation leads to a delay in the response of the same amount than the output pulse-width itself. This establishes a nonlinear dynamical basis for all-optical control of light, such as the realization of optical delay lines using arrays of coupled excitable PC microresonators.

We thank S. Barbay, R. Kuszelewicz, X. Letartre, P. Viktorovitch, and J. J. Greffet for helpful discussions.

*Electronic address: Alejandro.Giacomotti@lpn.cnrs.fr

[1] J. D. Murray, *Mathematical Biology* (Springer, New York, 1990).
[2] A. L. Hodgkin and A. F. Huxley, J. Physiol. **117**, 500 (1952); R. Fitzhugh, Biophys. J. **1**, 445 (1961); J. S. Nagumo, S. Arimoto, and S. Yoshizawa, Proc. IRE **50**, 2061 (1962).
[3] M. Giudici *et al.*, Phys. Rev. E **55**, 6414 (1997); A. M. Yacomotti *et al.*, Phys. Rev. Lett. **83**, 292 (1999); F. Marino *et al.*, Phys. Rev. Lett. **88**, 040601 (2002); H. J. Wunsche *et al.*, Phys. Rev. Lett. **88**, 023901 (2002).
[4] M. Larotonda *et al.*, Phys. Rev. A **65**, 033812 (2002); F. Plaza *et al.*, Europhys. Lett. **38**, 85 (1997).
[5] S. Barland *et al.*, Phys. Rev. E **68**, 036209 (2003).
[6] F. Marino *et al.*, Phys. Rev. Lett. **92**, 073901 (2004).
[7] V. Z. Tronciu and R. A. Abram, Phys. Rev. E **65**, 026616 (2002).
[8] F. Hoppensteadt and E. M. Izhikevich, *Weakly Connected Neural Networks* (Springer, New York, 1997).
[9] T. J. Johnson, M. Borselli, and O. Painter, Opt. Express **14**, 817 (2006).
[10] T. Carmon *et al.*, Phys. Rev. Lett. **94**, 223902 (2005).
[11] E. Kuramochi *et al.*, Appl. Phys. Lett. **88**, 041112 (2006).
[12] F. Raineri *et al.*, Opt. Lett. **30**, 64 (2005).
[13] A. M. Yacomotti *et al.*, Appl. Phys. Lett. **88**, 231107 (2006).
[14] X. Letartre *et al.*, J. Lightwave Technol. **21**, 1691 (2003).
[15] B. Ben Bakir *et al.*, Appl. Phys. Lett. **88**, 081113 (2006).
[16] A. M. Yacomotti *et al.*, Phys. Rev. Lett. **96**, 093901 (2006), and references therein.
[17] W. Lu, D. Yu, and R. G. Harrison, Phys. Rev. A **58**, R809 (1998).
[18] In our calculations we use $\alpha = 10$, obtained from the experimental results (see [16]).
[19] τ_{th} characterizes heat dissipation out of the confined mode in the InP membrane. In our system, this is mainly due to vertical diffusion and thermal conduction across the InP-SiO_2 contact.
[20] This value is close to the one determined from the experimental $I_{\text{in}} = 25$ kW/cm^2k, with $I_{\text{sat}} \sim 3$ MW/cm^2 determined from pump and probe measurement.